Photometric Color Calibration of the Joint Monitor-Camera Response Function

Tobias Elbrandt and Jörn Ostermann

Institut für Informationsverarbeitung
Leibniz Universität Hannover
Appelstraße 9A, 30167 Hannover, Germany
{elbrandt,ostermann}@tnt.uni-hannover.de
http://www.tnt.uni-hannover.de

Abstract. When recording presentations which include visualizations displayed on a monitor or with a video projector, the quality of the captured video suffers from color distortion and aliasing effects in the display area. A photometric calibration for the whole image can not compensate for these defects. In this paper, we present a per-pixel photometric calibration method that solves this problem. We measure the joint monitor-camera response function for every single camera pixel by displaying red, green, and blue screens at all brightness levels and capture them separately. These measurements are used to estimate the joint response function for every single pixel and all three color channels with the empirical model of response (EMoR). We apply the estimated response functions on subsequent captures of the display to calibrate them. Our method achieves a mean absolute error of about 0.66 brightness levels, averaged over all pixels of the image. The performance is also demonstrated with a calibration of a real captured photo, which is hardly distinguishable from the original.

1 Introduction

Recordings of presentations which are based on or make use of a computer monitor or digital video projector often suffer from bad image quality in the recorded presentation screen area. This is due to imperfect color reproduction, aliasing effects and low radiance in these regions. Hence, a calibration of the captured video signal is necessary.

The photometric calibration of cameras is the method to estimate the response function f as the relation between the image irradiance E captured in time t and measured as brightness B.

$$f(Et) = B \tag{1}$$

To calibrate a measured brightness B, the corresponding integrated image irradiance $I = Et$ has to be determined by

$$I = f^{-1}(B) \tag{2}$$

K.N. Kutulakos (Ed.): ECCV 2010 Workshops, Part II, LNCS 6554, pp. 41–49, 2012.

This type of camera image calibration is a vital topic, as it is a precondition for a lot of technology like image stitching, high dynamic range, shape-from-shading, and photometric stereo. Different approaches have been pursued to estimate the aforementioned relation, f. In most cases, parametric models, like gamma curves [1–3] or higher-order polynomials [4] are used. In contrast, a PCA based empirical model which generalizes the response functions of several real-world cameras was developed in [5]. Using a gamma function model gives an advantage, as it is inherently invertible whereas most other approaches make numerical means necessary to determine Eq. (2). Most of the methods only calibrate grayscale images, while [2] differentiates between different color channels.

The calibration of the monitor itself is an important issue for photographers, in order to make displayed photos match the captured ones. The gamma values needed to correctly display photographs taken by a consumer DSLR camera are determined in [6]. To provide a correctly proportional presentation of medical softcopy images, the monitor can be calibrated using a look-up-table measured with a luminance sensor [7].

Our goal is to compensate color distortions and Moiré effects, while capturing images from monitors. In this work, we will focus on the calibration of joint monitor-camera response functions, assuming that the method would be quite similar for a digital video projector. In order to get an understanding of the calibration procedure, we start with a concise description of the system. We divide the estimation of the combined monitor-camera response function in a pre-estimation of the monitor gamma, followed by an accurate estimation of the remaining camera response function for every single pixel, using the eigenvectors of the Empirical Model of Response (EMoR) database [5]. The performed experiments show that this two-step approach has good results. Finally, we apply the estimated calibration parameters to a real photograph. The last section concludes our paper.

2 Method for Calibrating the Joint Monitor-Camera Response Function

Our calibration method calibrates a camera that captures images from an LCD monitor. For this, a camera captures the monitor screen, filled with one of the three color channels, at different brightness levels. First, we analyze the used components, and then describe the calibration procedure.

2.1 Signal Generation and Reception

An ordinary LCD monitor provides a flat screen that can display color images consisting of three color planes – red, green, and blue. Normally, it also features a gamma curve, i.e. the light output is related exponentially to the displayed intensity value. There is always some additional low amplitude noise on the intensity. As the monitor also emits light when displaying only black pixels, the signal is biased. Every monitor pixel is divided into three sub-pixels, one for

each of the red, green, and blue color channels. When displaying white color, all sub-pixels are switched on, whereas when displaying green, the red and blue sub-pixels are blocked.

The camera maps light emitted by the monitor onto a two dimensional array of light sensitive camera pixels. In case of a single-chip color camera, which is commonly used, there is a color filter in front of every camera pixel, allowing only light within a certain bandwidth of the light spectrum to pass. The so called Bayer-pattern is the most widely-used sort of color filter arrays, with one red, two green, and one blue color filter for each 2×2 pixels. The passbands of the filters overlap a bit, such that the green pixels are also sensitive to the red and blue light spectrum. Some sources of noise between the reception of light and the output of digital values for the camera pixels add a bias and zero-mean noise [8]. While the signal output of every single camera element – apart from being quantized – is proportional to the gathered light, it is often adjusted by the camera to get better images for human eyes.

The combination of monitor and camera adds two effects that substantially influence the signal reception: Since the quantity of light emitted by the monitor pixels decreases with the angle of radiation, the incident light perceived by the camera depends on the viewing angle. Another effect is the Moiré, caused by aliasing due to the rasterization of both the LCD monitor and camera.

Figure 1 illustrates both effects in a graph showing brightness levels measured at adjacent red, green, and blue color elements of one image column, when the camera captured a red, green, and blue monitor screen, respectively. The aliasing causes the waves, while the angle dependent light emission is responsible for the respective base curve. Both influences on a real image can be observed in Fig. 4 a). It is also evident that the waves caused by the aliasing feature different phases. The phase shifts are due to the different spatial positions of both the monitor sub-pixels and the Bayer mosaic of the camera target elements for the three color channels. Comparing the curves of two diagonally adjacent green elements of the Bayer pattern (Fig. 1, right) shows that the aliasing component is rotated about 180° between them.

2.2 Two-Step Calibration Procedure

Considering the analysis above, we pursue the following strategy to calibrate the joint monitor-camera setup:

- Average several captured monitor images to minimize the influence of noise and quantization.
- Measure the response function separately for the base color channels as they measure overlapping bands of the light spectrum.
- Compensate the monitor's gamma separately, as it is not explicitly modeled by the camera response function.
- Calibrate the response function for every single pixel, as it greatly depends on the position.

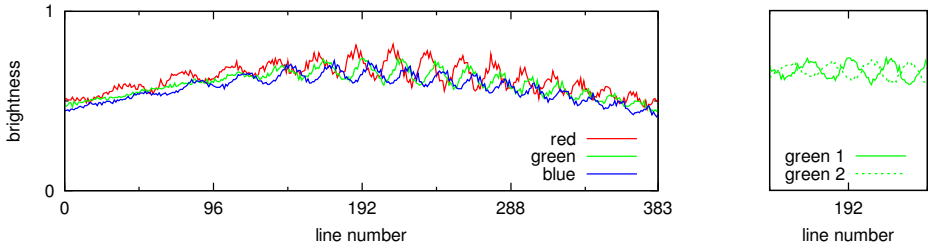

Fig. 1. Left: Brightness levels of the red, green, and blue camera image elements in one column when capturing a red, green, or blue screen, respectively. The Moiré effect is visible in the low amplitude waves, while the base curve shows the general angle dependent light perception. A calibrated camera would show lines with constant brightness levels. Right: The center part of the curves of the two green elements illustrates that the phase shift of the aliasing wave depends on the position of the camera target element.

Compensating the Monitor's Gamma: The **first step** of our method is to analyze and compensate the monitor's gamma. Assuming that both the monitor brightness f_m and the camera response function f_c approximately follow a gamma curve, we can combine both gammas. In addition to the signal biases β of the monitor and camera, this leads to the rough approximation Eq. (3) for the joint monitor-camera response function f_{mc} in relation to the integrated image irradiance I.

$$\begin{aligned} f_{mc}(I) = f_c(f_m(I)) &= \lambda_c \left(\lambda_m I^{\gamma_m}\right)^{\gamma_c} = \lambda I^{\gamma} \\ \text{with } \lambda = \lambda_c \lambda_m^{\gamma_c} &\text{ and } \gamma = \gamma_c \gamma_m \\ f_{mc}(I) &= \lambda I^{\gamma} + \beta \end{aligned} \tag{3}$$

We display red, green, and blue screens with increasing intensities i, and capture them N times each, as $\hat{C}_{c,i,n}(x,y) \in [0 \ldots 255]$, $c \in \{red, green, blue\}$, $i = 0 \ldots M\text{-}1$, $x = 0 \ldots w_c\text{-}1$, $y = 0 \ldots h_c\text{-}1$. The constants w_c and h_c denote the width and height of the camera target, respectively, and the perceived light intensities are quantized to 256 steps. All pixels of the images taken for an intensity are then averaged to the mean captured brightness

$$\hat{B}_c(i) = \frac{1}{w_c h_c N} \sum_{x,y} \sum_{n=1}^{N} \hat{C}_{c,i,n}(x,y). \tag{4}$$

Using these measurements, the parameter sets $\{\lambda, \gamma, \beta\}_c$ for all colors c are determined using a power regression with offset, i.e. the values for λ, γ, and β are estimated to minimize the error between the measurements $\hat{B}_c$ and Eq. (3).

The monitor is now set to the three gamma values calculated. This actually leads to an output signal of the camera, which is *on average*, approximately linear.

Estimating the Monitor-Camera Response Function: For the **second step**, the display-capture procedure described above is repeated, with the camera capturing the now gamma-calibrated monitor. Again, we measure pixel brightness $\hat{C}_{c,i,n}(x,y)$ which are now averaged to:

$$\hat{B}_{c,i}(x,y) = \frac{1}{N}\sum_{n=1}^{N} \hat{C}_{c,i,n}(x,y). \tag{5}$$

Therefore, we have measurements which describe what camera brightness $\hat{B}$ was received at pixel position (x,y), when the screen displayed the color c with intensity i. Depending on the type of the Bayer pattern of the camera, only 1 (red or blue) or 2 (green) measurements of each 2×2 pixels are taken into account. For example, our camera has an RGGB pattern, so we only regard measurements of the red images at positions where both x and y are even, and likewise, the data of the blue raw images are only regarded at positions where both x and y are odd. The green images are only taken into account at the two remaining positions. Hence, only one of three vectors $\hat{f}_c(x,y) = \{\hat{B}_{c,0}, \ldots, \hat{B}_{c,M-1}\}$ remains for each position.

We tested several methods to calibrate images per-pixel using the vectors $\hat{f}_c(x,y)$ and found that EMoR [5] outperformed the other techniques. Grossberg and Nayar unified 201 films and cameras to 25 PCA eigenvectors h_m and an average vector f_0. Using these vectors[1], the measurements $\hat{B}$ are approximated for all positions (x,y) and the respective color channel c with $H = [h_1 \ldots h_{25}]$:

$$a = H^{+}\left(\frac{\hat{B} - b_0}{b_1 - b_0} - f_0\right) \tag{6}$$

$$\tilde{B} = f_0 + Ha \tag{7}$$

Here, $H^{+} = \left(H^T H\right)^{-1} H^T$ is the Moore-Penrose inverse of H, and $b_0 = \min(\hat{B})$ and $b_1 = \max(\hat{B})$ are normalization coefficients to map $\hat{B}$ onto the interval $[0 \ldots 1]$. The first two coefficients a_1 and a_2 for the three color channels are shown in Fig. 2 a-c). Figure 2 d) shows the average vector f_0 and the two most significant eigenvectors h_1 and h_2.

Both the measurements $\hat{B}$ and the approximation $\tilde{B}$ provide camera picture brightness B against displayed intensity I on the screen, i.e. $f(I) = B$. In order to calibrate images, we have to invert this relation to $f^{-1}(B) = I$. This has to be done numerically, as no underlying invertible function is known for a linear combination of f_0 and h_i. Our calibration procedure therefore finishes with replacing the intensity of every camera pixel with the value of the corresponding inverted relation $\tilde{B}_c^{-1}(x,y)$. We also calibrated using the set of inverted EMoR PCA vectors $h_1^{\text{inv}}, \ldots, h_{25}^{\text{inv}}$, also provided by the authors.

[1] The vector data can be downloaded under `http://www.cs.columbia.edu/CAVE/software/softlib/dorf.php`

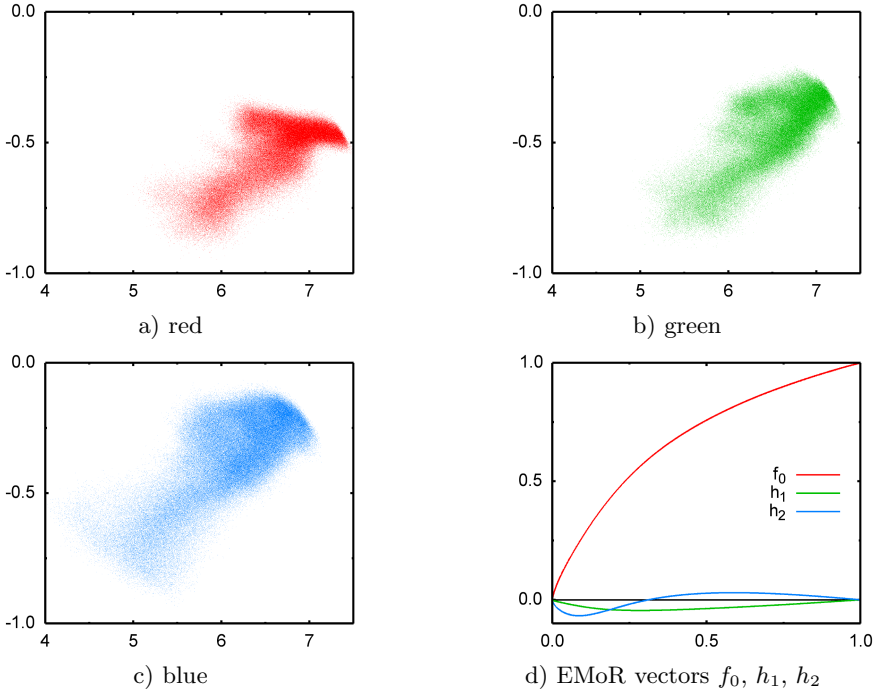

Fig. 2. Point-clouds of the distributions of the most significant coefficients a_1 and a_2 for the PCA vectors a calculated with Eq. (6) of the color channels a) red, b) green, and c) blue over all pixel positions. It can be observed that the coefficients vary greatly between pixels and color channels. This means that the resulting EMoR approximations diverge between different pixel positions. Fig. d) displays the EMoR average vector f_0 and the most significant vectors h_1 and h_2.

3 Experiments

For our experiments, we captured a Samsung 910T 19" TFT monitor with a Prosilica EC1380C FireWire camera. Both the brightness level of the monitor and the exposure time of the camera were adjusted, such that no signal clipping occurred.

In three loops, full-screen rectangles with increasing intensity from black to full amplitude were displayed on the monitor for the red, green, and bluecolor channels. Each of the screens was captured N=16 times and averaged to minimize noise effects, as well as quantization errors. For the first step, we obtained the measurements $\hat{B}_c(i)$. Their approximation with Eq. (3) resulted in the gamma values 2.02, 1.965, and 1.886 for the three channels. The monitor gamma was set to these values.

Then, we repeated the display-capture procedure to receive measurements $\hat{B}_{c,i}(x, y)$, which were then approximated to $\tilde{B}_c(x, y)$ using Eq. (6) and Eq. (7). To get another set of test data $\hat{B}'_{c,i}(x, y)$, this procedure was repeated again.

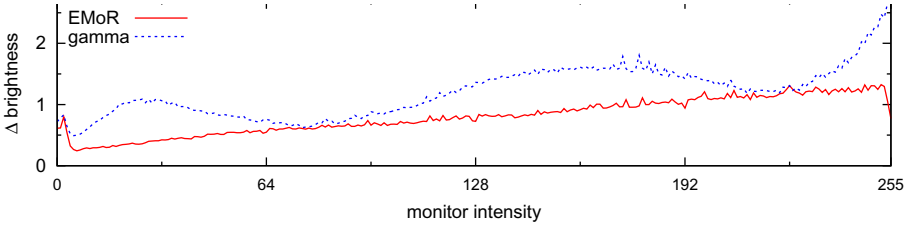

Fig. 3. Root mean square error of the calibration with EMoR and gamma approximation. The errors of both methods rise with increasing intensity level. Comparing the run of the error curve of the gamma approximation with the curves of h_1 and h_2, shown in Fig. 2 d), reveals a certain similarity; these small variations of the response functions from the gamma curve are also covered by EMoR.

We started our evaluation of the calibration procedure itself with ground-truth data. For this purpose, we took the values of the images $\hat{B}'_{c,i}(x,y)$ and calibrated them with $\tilde{B}_c(x,y)$. A perfect calibration should have the result i. The root mean square error (RMSE) between ground-truth i and the calibration results is shown in Figure 3. We included the corresponding graph for a calibration made with an approximated gamma curve; EMoR clearly outperforms the gamma based method, even though both methods are appropriate for our purposes. Table 1 summarizes and compares calibration errors for different techniques. We evaluated the calibrations both with and without a pre-gamma-corrected monitor (step one). The first line displays the results of calibration with per-pixel estimated gamma-curve. Using the measured values $\hat{B}_{c,i}$ directly as a look-up-table, results in the errors shown in the second line; although measured with averaged captures, they are still too noisy to be directly used. A calibration with the inverse EMoR vectors $h_1^{\text{inv}}, \ldots, h_{25}^{\text{inv}}$ is displayed in the second to last line. The direct inversion of the calibration with the approximated $\tilde{B}_{c,i}$ using the above mentioned EMoR vectors $h_1, \ldots, h_{25}$, outperformed the other methods.

After the calibration procedure, we want to show the outcome of our method. For this purpose, we displayed a photograph one color plane after another on the screen and captured it as raw images with the camera. The respective bayer pixels were extracted from each image, e.g. only the even pixel positions of the red capture. These were calibrated using our method, and again put together to

Table 1. Overall measurement of the errors of different calibration procedures. Displayed are the mean absolute error (MAE) and the root mean square error (RMSE) in brightness levels $[0 \ldots 255]$, for calibrations without or with compensation of the monitor's gamma (step one).

method	not gamma corrected		gamma corrected	
	MAE	RMSE	MAE	RMSE
gamma	2.419	3.119	1.103	1.426
look-up-table	0.928	2.213	0.740	1.012
EMoR inverse	1.107	2.558	0.679	0.913
EMoR direct	0.853	2.117	0.662	0.893

a) captured b) calibrated

Fig. 4. Photograph a) captured from the screen; the colors are dull and aliasing effects are evident in the colored waves. In the calibrated image b), both effects are compensated. Note that the image is still radially distorted.

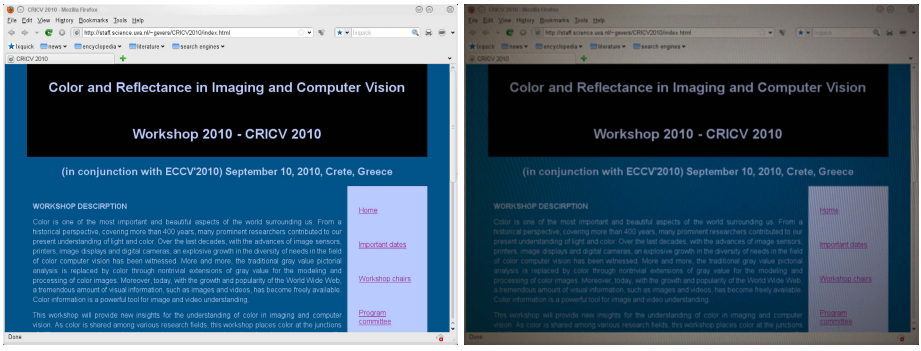

a) original b) de-calibrated

Fig. 5. The screen shot a) was blurred and then de-calibrated to get an appearance b) as if it was captured by a camera from the monitor

form a calibrated raw image, which was finally demosaiced. The result is shown in Fig. 4. Both the aliasing and color distortions are perfectly compensated.

For the authentic synthesis of scenes including a monitor, a realistic color distortion might be desired for the visible area of the screen. To make an image look like if it was captured by our camera from a monitor, we took a normal screen shot of a browser window (Fig. 5 a), added minor Gaussian blur, and *de-calibrated* it directly with $\tilde{B}_c(x, y)$. The result is shown in Fig. 5 b).

4 Conclusion

We presented a method to calibrate color images from a monitor screen that were captured by a camera. Our calibration procedure works in two steps. First, it estimates the gamma of the monitor, and then it approximates the camera

response curve using the EMoR model. Both estimations are performed using camera captures of the monitor, subsequently displaying different brightness levels. The mean absolute error achieved with our method is 0.662 intensity levels, with a root mean squared error of 0.893. With the calibration of a real captured photograph, we showed that undesirable effects, like Moiré and color distortion, are completely compensated.

References

1. Mann, S., Picard, R.W.: On being 'undigital' with digital cameras: Extending dynamic range by combining differently exposed pictures. In: Proceedings of IS&T, pp. 442–448 (1995)
2. Shafique, K., Shah, M.: Estimation of the radiometric response functions of a color camera from differently illuminated images. In: Proceedings of the IEEE International Conference on Image Processing, pp. 24–27 (2004)
3. Debevec, P.E., Malik, J.: Recovering high dynamic range radiance maps from photographs. In: SIGGRAPH, pp. 369–378. ACM (1997)
4. Mitsunaga, T., Nayar, S.: Radiometric self calibration. In: IEEE Computer Society Conference on Computer Vision and Pattern Recognition, vol. 1, pp. 374–380 (1999)
5. Grossberg, M., Nayar, S.: What is the space of camera response functions? In: IEEE Computer Society Conference on Computer Vision and Pattern Recognition, vol. 2, pp. II-602–II-609 (2003)
6. Manders, C., Mann, S.: True images: A calibration technique to reproduce images as recorded. In: Eighth IEEE International Symposium on Multimedia, ISM 2006, pp. 712–715 (2006)
7. Jiquan, L., Jingyi, F., Duchun, L.: Dicom GSDF based calibration method of general LCD monitor for medical softcopy image display. In: The 1st International Conference on Bioinformatics and Biomedical Engineering, ICBBE 2007, pp. 1153–1156 (2007)
8. Healey, G., Kondepudy, R.: Radiometric CCD camera calibration and noise estimation. IEEE Transactions on Pattern Analysis and Machine Intelligence 16 (1994)